Parallel to the spectrum analyser, an oscilloscope can be used for a check measurement. It is evident that for the purpose of measurement the RF current amplitude is substituted for by the bias current, which explains the name of RF DC substitution.

In practice, the measurement criterion of the appearance and disappearance of the modulation-frequency harmonics on both sides of the laser P/I characteristic has proved to be very well reproducible and feasible. However, the sensitivity of the receiver in conjunction with the spectrum analyser and/or the oscilloscope must be large enough to detect even the low AM voltage in the case of SD. Since this is a relative measurement procedure, no further extraordinary requirements have to be met by the receiver.

The measuring sensitivity is determined by the optical receiver and the subsequent spectrum analyser. In measurements using a spectrum analyser with a measuring bandwidth of 1 kHz and a broadband receiver (1·5 GHz) it was possible to detect even optical signals with an average power level of less than −75 dBm.

The described procedure is reliable only if the modulation current amounts to a multiple (by at least the factor 10) of the laser AM noise in the modulation-frequency range concerned.

Results: As an application example, the FM response was determined for a DFB laser of Nippon Electric Company (NEC) and one of the Research Institute of the Deutsche Bundespost (FI-DBP) (NEC: DC-PBH laser NDL 5650; FI-DBP: mushroom laser[5]). The current values required for this purpose were measured by means of the procedure described previously. The modulation frequencies ranged between 100 Hz and 560 MHz.

The curves shown in Fig. 3 illustrate clearly that the FM response is dependent on the modulation frequency. In the

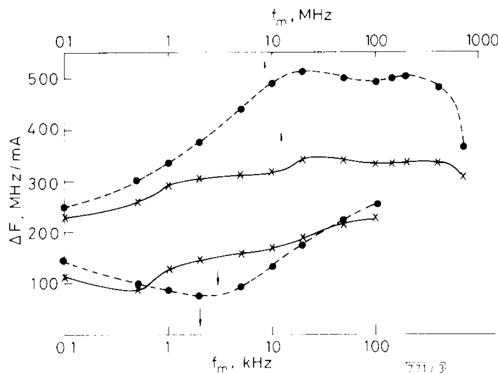

Fig. 3 *Measured FM response ΔF of two DFB lasers (MHz/mA)*

●●● DC laser of NEC

× × × mushroom laser of Research Institute of Deutsche Bundespost (FI-DBP)

kilohertz range the curves are determined by a thermal modulation of the refractive index, and by a modulation of the charge-carrier density above that range. For $f_m = 0$ (DC FM response) the FM response amounts to 190 MHz/mA and 405 MHz/mA for the NEC and the FI-DBP laser. Moreover, it can be seen that the FI-DBP laser has a flatter FM response than the NEC laser.

M. ROCKS
L. GIEHMANN

4th November 1988

Forschungsinstitut der DBP beim FTZ
Außenstelle Berlin
Ringbahnstrasse 130, D-1000 Berlin 42, Federal Republic of Germany

References

1 OLESON, H., and JACOBSEN, G.: 'Theoretical and experimental analysis of modulated laser fields and power spectra', *IEEE J. Quantum Electron.*, 1982, **QE-18**, pp. 2069–2080

2 ALEXANDER, S. B., and WELFORD, D.: 'Equalisation of semiconductor diode laser-frequency modulation with a passive network', *Electron. Lett.*, 1985, **21**, pp. 361–362

3 VODHANEL, R. S., and ENNING, B.: '1 Gbit/s bipolar optical FSK transmission experiment over 121 km of fibre', *ibid.*, 1988, **24**, pp. 163–164

4 MEINKE, GUNDLACH: 'Taschenbuch der Hochfrequenztechnik', Vol. 1. 4th edition, chapter 15 (Springer-Verlag, 1985)

5 BURKHARD, H.: 'Halbleiterlaser aus dem System InGaAsP/InP', Mitteilungen aus dem Forschungsinstitut der Deutschen Bundespost, (12), March 1988, pp. 45–99

MONOLITHIC PROGRAMMABLE RF FILTER

Indexing terms: Filters, Circuit theory and design

A voltage programmable monolithic continuous-time bandpass filter that employs transconductance-amplifier-based fully differential integrators is introduced. Experimental results of a circuit fabricated in a 3 μm CMOS process that is programmable over the range from 2 to 16 MHz are presented.

Introduction: Recently, several continuous-time high frequency filters have been reported in the literature.[1–3] These structures use the transconductance amplifier instead of a conventional op-amp to take advantage of the inherently better high frequency performance of the transconductance structures. Although the transconductance amplifier offers better high frequency performance than the op-amp, the performance of this device also deteriorates at high frequencies limiting the performance of reported monolithic filters employing these devices to a few megahertz. The major limitation in the high frequency performance of typical transconductance amplifier architectures is attributed to the limited bandwidth of internal current mirrors. Two groups have recently investigated simpler transconductance amplifiers in which the current mirror has been eliminated to improve the high frequency performance. Khorramabadi and Gray[1] use a single stage 'transconductor'. However, the lack of an active Q control scheme restricts the application of this structure to low Q filters. The dynamic range of this structure was modest and operation was limited to the 500 kHz range. More recently, Park and Schaumann reported[3] a 4 MHz bandpass filter using a CMOS inverter-like single stage transconductor. Although they were successful at improving the operating frequency range, the dynamic range was still quite limited.

In this paper, a new integrator structure is proposed which employs a CMOS inverter-based single stage fully balanced transconductor and the intrinsic capacitances of the MOS transistors. This structure operates at higher frequencies and offers improvements in dynamic range over existing schemes. Employing the proposed integrators, a programmable 16 MHz bandpass filter has been designed and fabricated in a 3 μm double metal CMOS process.

Design of a programmable integrator: A voltage controllable fully balanced transconductor-based integrator is shown in Fig. 1. Here, buffer transistors M7–M10 are used to lower the input capacitance, whereas the current sources M11–M12 are employed to adjust the bias currents in the load devices M3–M6. If the drain junction capacitances and parasitic capacitances associated with the buffer and current source transistors are neglected and if all transistor pairs are assumed to be matched, the transfer function of this integrator is approximately given by

$$\frac{V_0(s)}{V_i(s)} \simeq \frac{-g_{m_1}}{g_0 + sC_L} \quad (1)$$

where $g_0 = g_{m_3} - g_{m_5} + g_{ds_1} + g_{ds_3} + g_{ds_5}$ and $C_L \simeq C_{gs_3} + C_{gs_5} + C_{int}$. Here, g_{m_1}, g_{m_3}, g_{m_5} are transconductances, g_{ds_1}, g_{ds_3}, g_{ds_5} are output conductances, C_{gs_3} and C_{gs_5} are gate-source capacitances of the transistors, and C_{int} is the extrinsic integrating capacitor. For high frequency operation, C_{int} is

purposely omitted. g_{m_1} and g_0 control can be achieved by adjusting V_{f_0} and V_Q, respectively. It will be shown later that g_{m_1} and g_0 will serve as f_0 and Q control of a biquadratic filter structure.

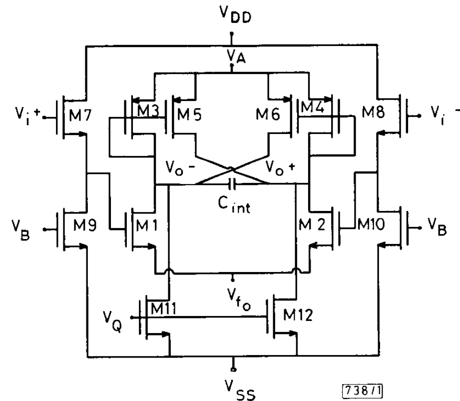

Fig. 1 *Schematic diagram of fully balanced integrator with control voltages*

Design of a tunable biquadratic filter: The block diagram of a fully differential integrator-based second-order filter which can utilise the integrator of Fig. 1 is shown in Fig. 2. This structure has both bandpass and lowpass outputs. The first and third stages are a lossy integrator and an ideal integrator

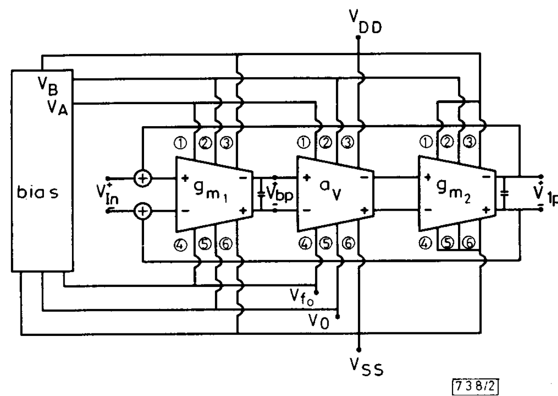

Fig. 2 *Block diagram of fully balanced integrator-based filter*

respectively implemented as previously described except for the following changes. Another buffer pair is used in the first stage integrator to provide a summing input for the feedback signal. In the third stage lossless integrator, the common sources of input devices, M1–M2, and those of the load devices, M3–M6 are connected to V_{DD} and V_{SS}, respectively, instead of to V_A and V_{f_0}.

The second stage is an inverting wide band amplifier which is used to provide common mode stability. The architecture of the wide band amplifier is basically the same as that of the integrator except for the inclusion of two ohmic load transistors which are small enough to guarantee a constant gain in the frequency range of interest. The voltage gain of this amplifier is dependent upon V_{f_0} and relatively independent of V_Q.

Neglecting the high frequency poles, the bandpass filter transfer function can be approximately derived as

$$A_v(s) \simeq \frac{-\alpha_{0_1} s}{s^2 + \omega_{p_1} s + a_v \alpha_{0_1} \alpha_{0_2}} \tag{2}$$

where α_{0_1}, α_{0_2} are the lossless unity gain frequencies of the first and third stage integrators, ω_{p_1} is the 3 dB frequency of the first stage integrator, and a_v is the gain of the second stage amplifier. The filter resonant frequency and the filter Q are given by

$$\omega_0 = \sqrt{(\alpha_v \alpha_{0_1} \alpha_{0_2})} \tag{3}$$

$$Q = \frac{\omega_0}{\omega_{p_1}} \tag{4}$$

The parameters α_{0_1} and α_v are used to set the filter resonant frequency, whereas Q is controlled by ω_{p_1}. In this filter structure, with the help of bias circuit, the DC operating point of each block is fixed at around zero regardless of the control voltages.

Experimental results: This filter was designed to have the nominal cut off frequency of 10 MHz, and a nominal Q of 10, and fabricated using a 3 μm CMOS double metal process. The output node is driven by an on-chip output buffer. The total chip area is $602 \times 495\,\mu m^2$. Excluding the buffer, the filter and bias circuitry require an area of $546 \times 170\,\mu m^2$. Tested with a ±5 volt power supply, the filter and bias circuitry consumed 69 mW of power. Fig. 3*a* shows the measured Q variation as a function of V_Q for the nominal f_0 of 10 MHz. The f_0 variation

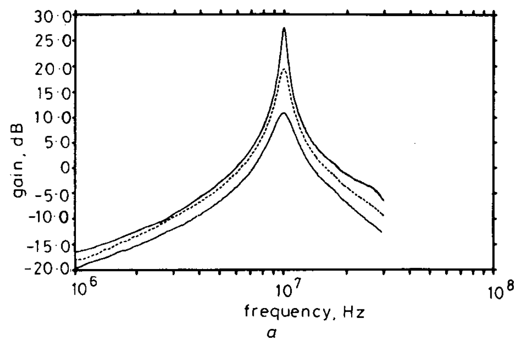

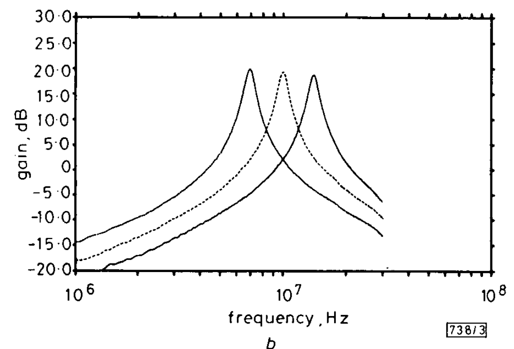

Fig. 3 *Measured variation in frequency response of bandpass filter*
a For constant f_0 = 10 MHz:
······· $Q = 5$ – – – – $Q = 10$ ——— $Q = 20$
b For constant $Q = 10$:
······· f_0 = 7 MHz – – – – f_0 = 10 MHz ——— f_0 = 14 MHz

as a function of V_{f_0} is exhibited in Fig. 3*b* for constant $Q = 10$. Experimental results exhibited a maximum output swing of 883 mV_{rms} at 1% THD with a total in band noise of 1·46 mV_{rms} and a corresponding dynamic range of 55·6 dB when programmed to operate with f_0 = 10 MHz and $Q = 10$. The centre frequency of this filter was adjustable through a range from 1·76 MHz to 16·86 MHz. A Q adjustable range of 0·5 ~ 68·9 was obtained.

Conclusions: A continuous-time high frequency monolithic filter has been implemented which operates at a nominal cut off frequency of 10 MHz and a Q of 10 using a new single stage transconductor-based integrator. It is shown experimen-

tally that wide control range for both cut off frequency and Q can be obtained with this technique.

T. G. KIM
R. L. GEIGER

2nd November 1988

Department of Electrical Engineering
Texas A&M University
College Station, TX 77843, USA

References

1 KHORRAMABADI, H., and GRAY, P. R.: 'High-frequency CMOS continuous-time filters', *IEEE J. Solid-State Circuits*, 1984, **CAS-33**, pp. 939–948
2 NEDUNGADI, A. P., and GEIGER, R. L.: 'High-frequency voltage-controlled continuous-time lowpass filter using linearised CMOS integrators', *Electron. Lett.*, 1986, **22**, pp. 729–731
3 PARK, C. S., and SCHAUMANN, R.: 'Design of an eighth-order fully integrated CMOS 4 MHz continuous-time bandpass filter with digital/analog control of frequency and quality factor'. Proc. Int. symp. circuits and systems, 1987, pp. 754–757

I/V ANOMALITY AND DEVICE PERFORMANCE OF SUBMICROMETRE-GATE $Ga_{0.47}In_{0.53}As/Al_{0.48}In_{0.52}As$ HEMT

Indexing terms: Semiconductor devices and materials, Microwave devices and components, Field-effect transistors

Discrepancies observed between the DC and RF characteristics of the $Ga_{0.47}In_{0.53}As/Al_{0.48}In_{0.52}As$ HEMT are presented. Owing to the deep-level electron trapping, the DC I/V curve is distorted and the DC transconductance (g_{mDC}) is severely compressed. The small-signal RF performance is not degraded by this low-frequency phenomenon. RF transconductance (g_{mRF}) of 555 mS/mm and the current gain cut-off frequency (f_t) of 102 GHz were obtained.

The superior electronic transport properties of the $Ga_{0.47}In_{0.53}As/Al_{0.48}In_{0.52}As$ lattice-matched HEMTs have been demonstrated in the high-speed and microwave device applications.[1–3] The anomalous current-voltage characteristics associated with these devices, often referred to as the kink effect, have been investigated and attributed to the electron traps in the AlInAs layers in both MESFETs[4] and HEMTs.[5,*] The unusual DC and the related RF characteristics are reported in this letter.

The $Ga_{0.47}In_{0.53}As/Al_{0.48}In_{0.52}As$ heterostructure was grown by MBE on the semi-insulating InP substrate with the following growth sequence: *i*-AlInAs buffer layer/*i*-GaInAs channel/*i*-AlInAs spacer layer/n^+-AlInAs electron supplying layer/*i*-AlInAs barrier layer/n^+-GaInAs cap layer (2500 Å/500 Å/33 Å/200 Å/100 Å/100 Å). The n^+-AlInAs layer is doped to $4.5 \times 10^{18}/cm^3$ and the cap layer has a doping level of $6 \times 10^{18}/cm^3$. Hall measurement shows a room temperature electron mobility of 10 300 cm^2/V-sec and a sheet concentration of $2.87 \times 10^{12}/cm^2$.

Device fabrication started with the boron ion implantation isolation, which was followed by the ohmic level contact lithography and evaporation of Ni/AuGe/Ag/Au ohmic metals. Alloying was done in a rapid thermal annealer. T-shaped gate patterns with submicrometre footprints were defined by electron beam lithography. A recess etch was performed to place the Ti/Pd/Au gate directly on the undoped AlInAs barrier layer.

Shown in Figs. 1 and 2 are examples of the abnormal I/V curves at 300 K and at 77 K in the light and dark. Two anomalities are noted in such devices. First, kinks are present at a V_D ranging from 0·4 to 0·6 V similar to the previous reported

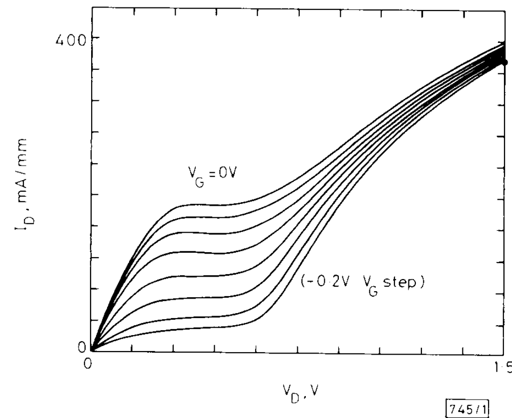

Fig. 1 *I/V characteristics of device 43 at 300 K*

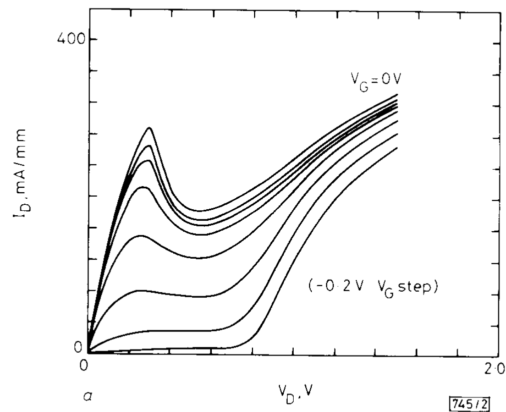

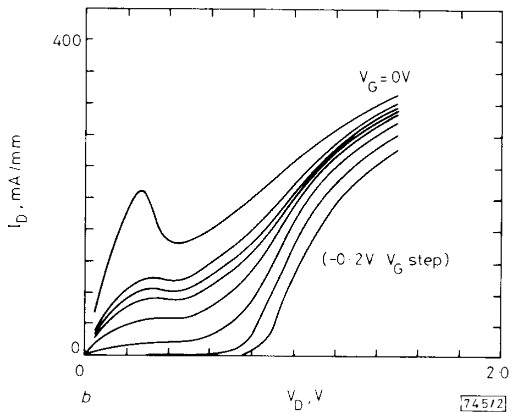

Fig. 2
a I/V characteristics of device at 77 K in the light
b I/V characteristics of device at 77 K in the dark

data.[4,5] Secondly, an abrupt increase of I_D with saturating trend for very negative V_G and large V_D was observed, which, in fact, severely degraded g_{mDC}.

Schottky gates were negatively biased during the measurement, and were confirmed to be working effectively by monitoring the gate current (in the microampere range and lower). There was no high-field, high-frequency instabilities, and no gate current conduction due to the real-space-transferred electrons. Measured S_{22} are less than 1. This then excludes one possible reason for generating such negative differential resistance in the drain I/V curves. Measurement was carefully per-

* PALMATEER, L. F., TASKER, P. J., SCHAFF, W. J., NGUYEN, L. D., and EASTMAN, L. F.: 'DC and RF measurement of the output conductance in a 0·2 µm gate length AlInAs/GaInAs/InP MODFETs', submitted to *IEEE Electron. Device Lett.*